

A-Priori Analysis of Conditional Moment Closure Modeling of a Temporal Ethylene Jet Flame with Soot Formation Using Direct Numerical Simulation

David O. Lignell^{a,*}, John C. Hewson^b, Jacqueline H. Chen^a

^a*Combustion Research Facility, Sandia National Laboratories, Livermore, CA, USA*

^b*Sandia National Laboratories, Albuquerque, NM, USA*

Abstract

Modeling soot formation in turbulent nonpremixed combustion is a difficult problem. Unlike most gaseous combustion species, soot lacks a strong state relationship with the mixture fraction due to unsteady formation rates which overlap transport time scales, and strong differential diffusion between gaseous species and soot. The conditional moment closure model (CMC) has recently been applied to the problem of turbulent soot formation. A challenge in CMC modelling is the treatment of differential diffusion. Three-dimensional direct numerical simulation (DNS) of a nonpremixed ethylene jet flame with soot formation has been performed using a nineteen species reduced ethylene mechanism and a four-step, three-moment, semi-empirical soot model. The DNS provides full resolution of the turbulent flow field and is used to perform a-priori analysis of a recent CMC model derived from the joint scalar PDF transport equation. Unlike other approaches, this CMC model does not require additional transport equations to treat differentially diffusing species. A budget of the terms of the CMC equation for both gaseous species and soot is presented. In particular, exact expressions for unclosed terms are compared to typical closure models for scalar dissipation, cross dissipation, differential diffusion, and reactive source terms. The differential diffusion model for gaseous species is found to be quite accurate, while that for soot requires an additional model for the residual term.

Keywords: CMC, DNS, nonpremixed flame, ethylene, soot

1. Introduction

Modeling and simulation of soot formation in turbulent flames is a problem of important practical and theoretical interest. Soot is formed in hydrocarbon flames in fuel-rich regions where insufficient oxygen is present to fully convert fuel to products. Soot emission results in reduced combustion efficiency in devices such as engines, and is an air pollutant. The majority of heat transfer from sooting flames and fires arises from the presence of soot in high temperature flame zones. A sound physical understanding of soot formation in turbulent flames and the ability to accurately model the phenomenon is important for quantitative design and optimization of combustion equipment, and analysis and prediction of fire hazards.

Turbulent soot formation is a challenging problem as soot chemistry is complex (making universal chemical mechanisms difficult to create and

computationally expensive to use). The optical thickness of sooting flames makes experimental measurements of detailed turbulent soot-flame structure difficult, and presently, only statistical quantities such as means and variances are experimentally available in sooting flames. Soot is a particle phase with a low diffusivity, resulting in thin structures and strong differential diffusion between soot and gaseous species. Unlike many nonpremixed hydrocarbon flames of practical importance, modeling soot formation in turbulent flames is complicated by the lack of a strong state relationship between soot and the mixture fraction. This problem arises from history effects associated with soot formation and growth rates with timescale overlap between reactive and transport processes. In addition, as noted, low soot diffusivity results in strong differential transport of soot in the mixture fraction coordinate.

The conditional moment closure (CMC) model solves unsteady transport equations for reactive scalars that are conditionally averaged on given values of mixture fraction [1, 2]. The conditional

*Corresponding Author; Tel.: (925) 294-6615; Fax: (925) 294-2595
E-mail: david@crsim.utah.edu

mean scalars, along with a description of the mixture fraction PDF allows a solution of the mean flow. This conditioning allows more accurate closure of nonlinear reactive source terms. Kronenburg and Bilger [3] have developed a CMC formulation allowing for differential diffusion (DD) of chemical species, but requiring solution of additional transport equations to solve for restorative terms associated with differential diffusion. This CMC approach accounting for DD was extended to soot formation in turbulent nonpremixed methane flames [4], and recently applied to turbulent nonpremixed ethylene flames [5]. In both cases, good agreement between simulation and experiment was observed, whereas significant under prediction of soot concentration resulted from neglecting DD. Hewson et al. [6] have recently presented a new CMC formulation for soot formation accounting for effects of DD that does not require the solution of additional transport equations, which significantly reduces computational costs. The CMC formulation was tested a-priori using one-dimensional turbulence results applied to a pool fire configuration.

We have performed three-dimensional direct numerical simulation (DNS) of a nonpremixed, temporal, planar ethylene jet flame with soot formation. Complex combustion chemistry, and a three-moment, four-step, semi-empirical soot model were employed with high spatial resolution. Detailed results of the simulation focusing on turbulent soot formation and differential transport between soot and mixture fraction are presented in Ref. [17]. In this paper, we use the DNS results to perform an a-priori study of the CMC equations developed by Hewson et al. [6]. A budget of terms in the CMC equations is presented for both gaseous and soot species. Exact expressions for unclosed terms are compared to possible closure models for these terms using conventional modelling assumptions.

2. DNS of the Turbulent Ethylene Flame

The DNS was performed using the code S3D, developed at Sandia National Laboratories. S3D solves the reacting Navier-Stokes equations using an explicit, low-storage, fourth-order Runge Kutta method for time integration [7]. Spatial derivatives are approximated with eighth-order central differences, and a tenth-order filter is applied to remove any aliasing errors [8]. Property dependent thermodynamic quantities are computed using Chemkin [9], and species diffusion fluxes are computed with a mixture averaged formulation using Transport [10].

A reduced ethylene mechanism was developed from a detailed mechanism using directed relation

graph methods, sensitivity analysis, and computational singular perturbation. The mechanism was extensively validated for all conditions experienced in the DNS, and consists of 19 transported species, 10 quasi-steady-state species, and 167 reactions. See [11] for details.

The soot model is based on the Leung and Lindstedt model [12], which has been used extensively in simulation of turbulent sooting flames. The model consists of four steps: nucleation, growth, oxidation, and coagulation. The gaseous nucleation and growth species is acetylene, C_2H_2 , and oxidation is written in terms of the oxygen concentration. The soot particle size distribution (PSD) is modeled using the method of moments. The first three mass moments of the PSD are transported, and closure of fractional moments is performed by assuming a lognormal size distribution [13]. The soot model is fully coupled with the gas phase in terms of the mass and energy conservation. Soot transport occurs primarily through thermophoresis, although Brownian diffusion is also implemented [11].

Radiative heat transfer is simulated using the optically thin model. The DNS length and time scales are not sufficient to involve significant radiative heat losses, and the optically thin model is adequate.

The three-dimensional flow configuration is a planar slot jet, with periodic boundary conditions in the streamwise (hence the jet is temporally-evolving) and spanwise directions. Nonreflecting outflow boundary conditions are applied in the cross-stream direction [14]. This configuration is physically important and practically relevant. The periodicity in two dimensions gives two directions of statistical homogeneity, and the temporal evolution maximizes the residence time of soot in the domain for unsteady growth. Table 1 shows the jet configuration parameters. In this table, H is the initial height of the jet, ΔU is the velocity difference between the interior fuel jet and the surrounding oxidizer stream, u' and L_{11} are the velocity fluctuation and integral scale of homogeneous isotropic turbulence imposed in the fuel core to trip the turbulent shear layers. $L_{x,y,z}$ are the domain lengths. A 30 micron grid spacing was used and found to adequately resolve all gaseous combustion species and velocity fields. The simulation was run for a total of 50 characteristic jet times. The nonpremixed flame is initialized using a steady laminar flamelet solution matching an imposed hyperbolic transition (with characteristic width δ_ξ) between the fuel and oxidizer streams [11]. The stoichiometric mixture fraction is 0.25, and is achieved by moving nitrogen from the air stream to the fuel stream. Both fuel and oxidizer

Table 1: Temporal ethylene jet simulation parameters.

H (mm)	1.8	L_x/H	16	τ_{jet} (ms)	0.022
ΔU (m/s)	82	L_y/H	11	τ_{run}/τ_{jet}	50
Re_{jet}	3700	L_z/H	6	# Cells	228×10^6
$u'/\Delta U$	4%	Δx (μm)	30	Sim. Cost (cpuh)	1.5×10^6
H/L_{11}	3	δ_ξ (mm)	0.8		

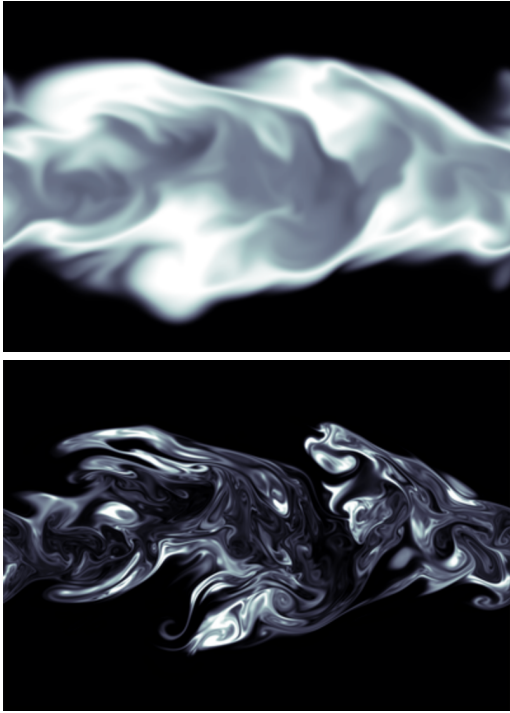


Figure 1: Isocontours, corresponding to a spanwise slice, of temperature (top) and Y_{soot} (bottom) at $t = 50\tau_j$. The peak Y_{soot} is off scale at 4.5×10^{-4} , located at $x = 0.72$ cm in the center region.

streams are preheated to 550 K.

Figure 1 shows contour plots of the temperature and soot mass fraction fields at the end of the simulation. The temperature field shows significant turbulence-flame interaction. The soot mass fraction has a low diffusivity, and shows thin structures as the soot is strained and convected by the turbulent flow. Soot is formed on the rich side of the flame, and convected by turbulent eddies into the fuel-rich core. The other two soot moments show a similar structure.

Scatter plots of temperature and mass fractions of soot, and C_2H_2 are shown in Fig. 2. Also shown in the figure are the conditional means and standard deviations of the quantities. The temperature, and C_2H_2 species show a relatively small degree of scatter, and a tight state relationship with the mixture fraction, as evidenced by the condi-

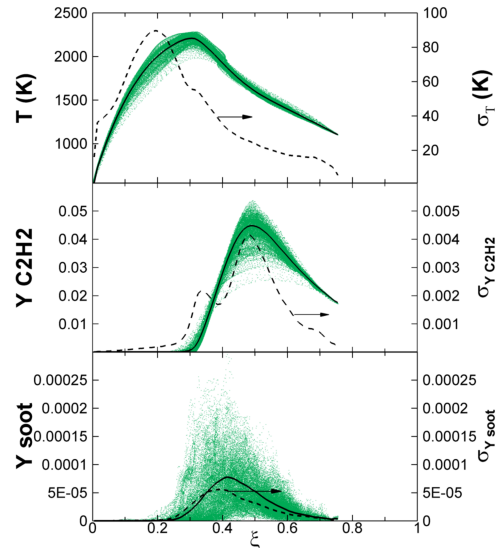


Figure 2: Scatter plots with conditional means and conditional standard deviations at $t = 50\tau_j$.

tional standard deviation having values an order of magnitude lower than the conditional mean. The conditional standard deviation of the soot mass fraction, by contrast, is of the same magnitude as the conditional mean. At the $t = 50\tau_j$ time shown, the peak mixture fraction is just below 0.8. The soot mass fraction peaks at $\xi = 0.4$, as does the soot reaction source terms. However, soot is present at nearly all mixture fractions greater than this (up to the maximum), in the simulation. The dispersion of soot towards higher mixture fractions occurs through differential diffusion between soot and gaseous species. Modeling this differential diffusion is the primary challenge of CMC of sooting flames.

3. CMC Formulation

The CMC equations considered in this paper are derived from the joint species PDF following Klimenko [1]. In the present simulation, the jet time scales are small enough that relatively low concentrations of soot are present, and there is no significant mass transfer between the gas and soot

phases. Hence, for the present purposes, the mixture fraction is computed from the gaseous mixture using Bilger's definition [15]. We also neglect the dependence of conditional quantities on the nonhomogeneous cross-stream direction (as is common in CMC modeling [4, 16]), so that all spatial derivatives of conditional quantities are neglected.

A brief description of the CMC model derivation is presented below. One begins by taking the average of the transport equation for the multi-dimensional fine-grain PDF by integrating over the multi-dimensional sample space to obtain the joint PDF transport equation. The transport equation for the fine grain PDF is given by

$$\begin{aligned} \frac{\partial \rho \psi}{\partial t} + \nabla \cdot (\rho \vec{v} \psi) + \frac{\partial}{\partial Z_i} (\psi \nabla \cdot (\rho D_i \nabla Y_i)) = & (1) \\ - \frac{\partial}{\partial Z_i} (\rho \psi w_i) - \frac{\partial}{\partial Z_i} (\psi \nabla \cdot (\rho^{-1} D_{T,i} Y_i \nabla \ln T)) \end{aligned}$$

Here, ψ is the fine grain PDF, w_i is a reaction source term, ρ is density, \mathbf{v} is velocity, T is temperature, D is a diffusivity, Y_i is a species random variable (including mixture fraction and soot mass-moments divided by density), and Z_i is its sample space variable. Index notation is used (but D_i refers directly to Y_i with no implied summation). The last term is the thermophoretic term and is assumed zero for all species except soot moments. The third term is the diffusion term, and is rearranged significantly in the derivation.

The diffusive term is split into two terms: a term with all diffusivities equal, and a correction to this:

$$\begin{aligned} \frac{\partial}{\partial Z_i} (\psi \nabla \cdot (\rho D_i \nabla Y_i)) = \frac{\partial}{\partial Z_i} (\psi \nabla \cdot (\rho D \nabla Y_i)) + & (2) \\ \frac{\partial}{\partial Z_i} (\psi \nabla \cdot (\rho (D_i - D) \nabla Y_i)) \end{aligned}$$

The derivation then proceeds as in the constant diffusivity case, and the correction term is brought along directly, with no additional rearrangement. The first term on the right hand side (RHS) is replaced according to the identity

$$\begin{aligned} \frac{\partial}{\partial Z_i} (\psi \nabla \cdot (\rho D \nabla Y_i)) = & (3) \\ \frac{\partial}{\partial Z_i} \frac{\partial}{\partial Z_j} (\psi \rho D \nabla Y_i \cdot \nabla Y_j) - \nabla \cdot (\rho D \nabla \psi) \end{aligned}$$

The term on the far RHS of this equation is replaced with the identity

$$\nabla \cdot (\rho D \nabla \psi) = \nabla^2 (\rho D \psi) - \nabla \cdot (\psi \nabla (\rho D)) \quad (4)$$

The resulting equation is averaged over the sample space to obtain the joint PDF transport equation:

$$\begin{aligned} \frac{\partial \langle \rho | \mathbf{Z} \rangle P}{\partial t} + \nabla \cdot (\langle \rho \vec{v} | \mathbf{Z} \rangle P) = - \frac{\partial}{\partial Z_i} (\langle \rho w_i | \mathbf{Z} \rangle P) & (5) \\ - \frac{\partial}{\partial Z_i} (\langle \nabla \cdot (\rho^{-1} D_{T,i} Y_i \nabla \ln T) \rangle P) \\ - \frac{\partial}{\partial Z_i} (\langle \nabla \cdot (\rho (D_i - D) \nabla Y_i) | \mathbf{Z} \rangle P) \\ - \frac{\partial}{\partial Z_i} \frac{\partial}{\partial Z_j} (\langle \rho D \nabla Y_i \cdot \nabla Y_j | \mathbf{Z} \rangle P) \\ + \nabla^2 (\langle \rho D | \mathbf{Z} \rangle P) - \nabla \cdot (\langle \nabla (\rho D) | \mathbf{Z} \rangle P) \end{aligned}$$

The terms on the RHS are a reaction term, a thermophoretic diffusion term, a DD correction term, a diffusion term and two terms arising from the diffusion term (which are normally neglected at high Reynolds number [1]).

The joint PDF equation is multiplied by one of the Z_i (say Z_k) and integrated over all Z_i except for η , where η is the sample space variable for mixture fraction, ξ . This results in the transport equation for conditionally averaged scalars, the CMC equation. Here, the identity of the diffusivity D must be determined, and different results are obtained with different choices. Setting D equal to the thermal diffusivity is a popular choice. Hewson et al. [6] set D equal to the species under consideration (that is $D = D_i$ corresponding to Z_k). The resulting equation for soot mass fraction is

$$\begin{aligned} \frac{\partial \langle \rho Y_s | \eta \rangle P_\eta}{\partial t} + \nabla \cdot (\langle \rho Y_s \vec{v} | \eta \rangle P_\eta) = \langle \rho w_{Y_s} | \eta \rangle P_\eta & (6) \\ + \langle \nabla \cdot (\rho Y_s D_{T,i} \nabla \ln T) | \eta \rangle P_\eta \\ - \frac{\partial}{\partial \eta} (\langle \nabla \cdot [\rho (D_\xi - D_s) \nabla \xi] Y_s | \eta \rangle P_\eta) \\ - \frac{\partial^2}{\partial \eta^2} (\langle \rho D_s (\nabla \xi)^2 Y_s | \eta \rangle P_\eta) \\ + \frac{\partial}{\partial \eta} (\langle 2 \rho D_s (\nabla Y_s \nabla \xi) | \eta \rangle P_\eta) \\ + \nabla^2 (\langle \rho D_s Y_s | \eta \rangle P_\eta) - \nabla \cdot (\langle \nabla (\rho D_s Y_s) | \eta \rangle P_\eta) \end{aligned}$$

This equation is a conservative form of the conditional transport equation for soot and is amenable to finite-volume discretization solution procedures [18]. The product $\langle \rho | \eta \rangle P_\eta$ is a density in the \vec{x} - η space and conversion between conservative and nonconservative forms is made using the mixture fraction PDF transport equation. Equation (6) can be rewritten in terms of other chemical species mass fractions instead of soot, by a simple change of notation, and by ignoring the thermophoretic term. When soot is considered, its diffusivity is so

small that terms multiplying D_s can be neglected. In that case, the differential diffusion term has the form

$$\frac{\partial}{\partial \eta} (\langle \nabla \cdot [\rho D_\xi \nabla \xi] Y_s | \eta \rangle P_\eta) = -\frac{\partial}{\partial \eta} (\langle Y_s \rho |\nabla \xi| v_\xi | \eta \rangle P_\eta) \quad (7)$$

Here, the quantity $|\nabla \xi| v_\xi$ is a diffusion velocity in the mixture fraction coordinate and appears below in Eqs. (8, 11). The differential diffusion term is physically the divergence of soot mass flux in the mixture fraction coordinate. The quantity v_ξ is the velocity of isocontours of mixture fraction normal to themselves, relative to the fluid velocity, and is defined as $v_\xi = -\frac{\nabla \cdot (\rho D_\xi \nabla \xi)}{\rho |\nabla \xi|}$. Here it is observed that the differential diffusion of soot is associated with this mixture fraction diffusion velocity, which has recently been studied in DNS of soot formation [11, 17].

Most of the terms in Eq. (6) are unclosed. In this paper, we compare the magnitudes of the terms on the RHS of Eq. (6), along with closure models for three of these terms. Following the primary closure hypothesis of Klimenko and Bilger [1], closures of the differential diffusion (DD) term, the dissipation-scalar (DS) term, and the cross-dissipation (CD) term, (which are terms 3, 4, and 5, respectively, on the RHS of Eq. (6)), are obtained [6]:

$$DD : -\frac{\partial}{\partial \eta} (\langle \nabla \cdot [\rho (D_\xi - D_s) \nabla \xi] Y_s | \eta \rangle P_\eta) \quad (8)$$

$$\approx -\frac{\partial}{\partial \eta} \left[\left(1 - \frac{1}{Le_{s,\eta}} \right) \rho_\eta M_\eta Q_s P_\eta \right]$$

$$DS : -\frac{\partial^2}{\partial \eta^2} (\langle \rho D_s (\nabla \xi)^2 Y_s | \eta \rangle P_\eta) \quad (9)$$

$$\approx -\frac{\partial^2}{\partial \eta^2} \left(\frac{\rho_\eta \chi_\eta Q_s}{2Le_{s,\eta}} P_\eta \right)$$

$$CD : \frac{\partial}{\partial \eta} (\langle 2\rho D_s (\nabla Y_s \nabla \xi) | \eta \rangle P_\eta) \quad (10)$$

$$\approx \frac{\partial}{\partial \eta} \left(\frac{\rho_\eta \chi_\eta}{Le_{s,\eta}} \frac{\partial Q_s}{\partial \eta} P_\eta \right)$$

In these equations, a subscript η is short for $\langle \cdot | \eta \rangle$, Q_s denotes the conditional mass fraction of soot, (or other species), and M_η is defined as

$$M_\eta = \frac{1}{\rho_\eta} \langle \nabla \cdot \rho D_\xi \nabla \xi | \eta \rangle \quad (11)$$

Klimenko and Bilger [1] provide the following expression relating M_η to χ_η :

$$M_\eta = \frac{1}{2\rho_\eta P_\eta} \frac{\partial (\rho_\eta P_\eta \chi_\eta)}{\partial \eta} \quad (12)$$

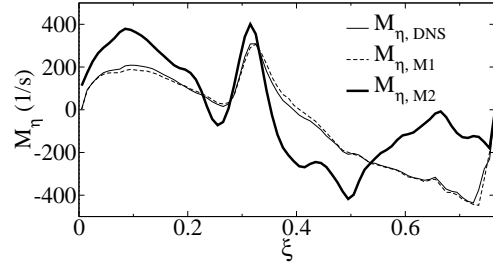


Figure 3: Comparison of M_η from Eq. (11), DNS, Eq. (12), M1, and $M_\eta = \frac{1}{2} \frac{\partial \chi_\eta}{\partial \eta}$, M2 at $t = 50\tau_j$.

Yunardi et al. [5] approximated this equation with $M_\eta = \frac{1}{2} \frac{\partial \chi_\eta}{\partial \eta}$ by neglecting the η dependence of $\rho_\eta P_\eta$. Following the approach discussed below in Section 4, Fig. 3 compares this approximation with M_η from Eqs. (11, 12). Equation (12) is in very close agreement with the unclosed expression from the DNS, whereas the approximation $M_\eta = \frac{1}{2} \frac{\partial \chi_\eta}{\partial \eta}$ shows significant error; the relative mean errors are 6.5%, and 77%, respectively.

4. Results

The CMC terms, unclosed in Eq. (6), and closed in Eqs. (8-10) were evaluated from the raw DNS data by conditionally averaging using 100 bins in the mixture fraction coordinate. The conditional data are relatively smooth, but derivatives, especially second derivatives are very noisy. A filter that removes high wavenumber content containing little energy was applied to the raw conditional data for which derivatives in the mixture fraction coordinate were taken.

4.1. Soot Mass Fraction Equation

Figure 4 shows a comparison of three key terms on the RHS of Eq. (6) for the soot mass fraction at times of $t = 25\tau_j$ and $t = 50\tau_j$. The terms shown are the reaction source term, the differential diffusion term, and the thermophoretic diffusion term. Spatial derivatives of conditional mean quantities are not considered, and the soot diffusivity is equal to zero. The magnitude of the terms at the later time is higher because the PDF of the mixture fraction is higher in the reactive regions as the combustion products expand and fuel and oxidizer mix. In addition, the peak $\langle Y_s \rangle$ at $t = 50\tau_j$ is approximately five times the value at $t = 25\tau_j$. At a given time, the reaction and differential diffusion terms are of similar magnitudes, showing the importance of both terms. The thermophoretic term, however has a much smaller magnitude and this term does not contribute significantly to the conditional soot transport equation. These results

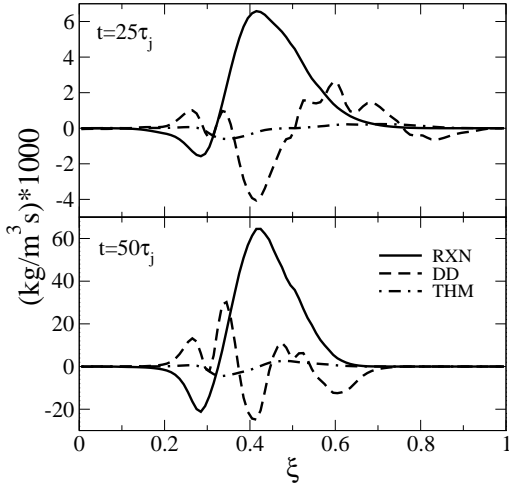


Figure 4: CMC terms for conditional soot mass fraction equation at two times.

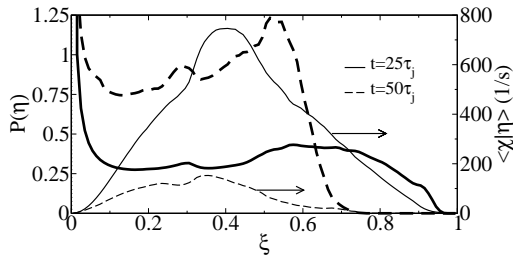


Figure 5: PDF of mixture fraction (bold lines), and conditional mean scalar dissipation rate (thin lines) at two times.

are consistent with comparisons between the diffusive velocity of the mixture fraction and thermophoretic diffusion velocity [11, 17].

The dual peaks in the differential diffusion term near the stoichiometric point arise from a small peak in the mixture fraction PDF at this point. Near this location, flow dilatation and temperature (hence kinematic viscosity) are high and the local Reynolds number is low, reducing mixing rates. This peak coincides with a depression in the conditional mean scalar dissipation rate. The mixture fraction PDF and conditional mean scalar dissipation rate are shown in Fig. 5.

Figure 6 shows the differential diffusion term for soot mass fraction, as well as the model approximation for this term, given in Eq. (8). The DD term and its model are of similar magnitudes overall. The agreement between the two terms is good at very rich mixture fractions. However, at intermediate mixture fractions, and near the flame zone, large differences exist. Hewson et al. [6] noted this discrepancy and proposed a model for the residual DD term, representing the error between the exact term and its modeled approximation. The model is based on a turbulent diffusion

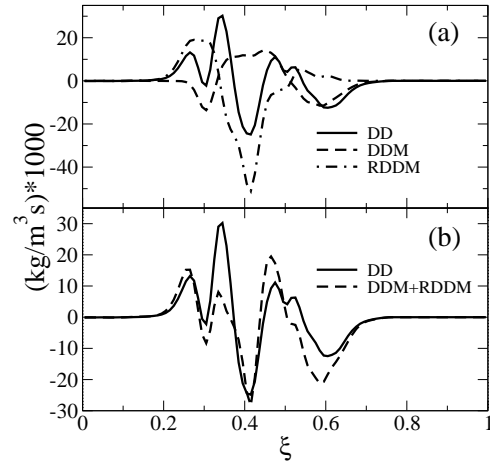


Figure 6: Plots of differential diffusion term and its models for the soot mass fraction CMC equation at $t = 50\tau_j$.

process in mixture fraction space and is given by

$$RDDM \approx \frac{\rho_\eta \chi_\eta P_\eta}{2Le_{DD,t}} \frac{\partial^2 Q_s}{\partial \eta^2}, \quad (13)$$

where $Le_{DD,t}$ is an effective turbulent Lewis number. The RDD term is also plotted in Fig. 6 (a), as the dash-dot line. In Fig. 6 (b), the DD term is plotted along with the sum of the modeled, and modeled residual DD terms. Here $Le_{DD,t}$ was arbitrarily set to a value of 3.0 to give reasonable quantitative agreement between the curves. The sensitivity of this model parameter to the flow and combustion configuration (e.g., Reynolds number) is unknown and requires further investigation. The sum of the model and residual terms is observed to reproduce the qualitative shape of the exact DD term throughout the whole mixture fraction domain. The quantitative agreement is also remarkably good, consistent with previous results [6].

4.2. Gaseous Species

The CMC transport equation Eq. (6) is applicable to gaseous species as well as soot, with a change of notation: D_s and Y_s refer now to the species mass fractions instead of soot mass fractions. Whereas the soot diffusivity is practically zero, the species diffusivities are significant, and the fourth and fifth terms on the RHS of Eq. (6) are present in the balance equation. The thermophoretic term is neglected for gaseous species, however.

The upper plots of Figs. 7, 8, and 9 show the exact CMC terms of Eq. (6) for reactive scalars CO_2 , OH , and H at $t = 50\tau_j$. For each gaseous species, the four terms shown are of similar magnitudes in all regions of the mixture fraction coord-

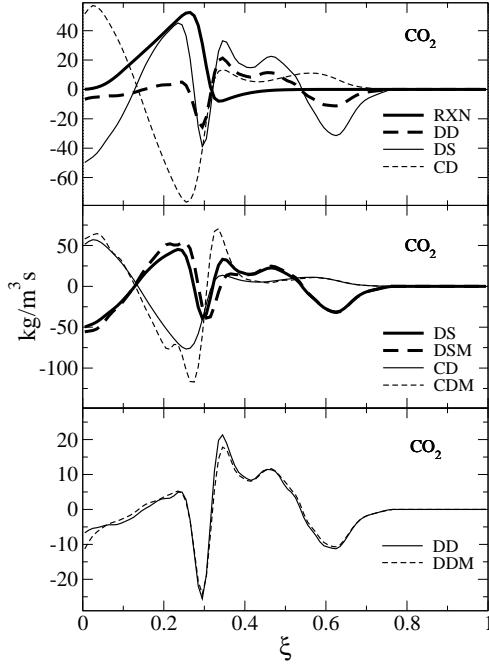


Figure 7: Plots of exact and modeled CMC terms for CO_2 .

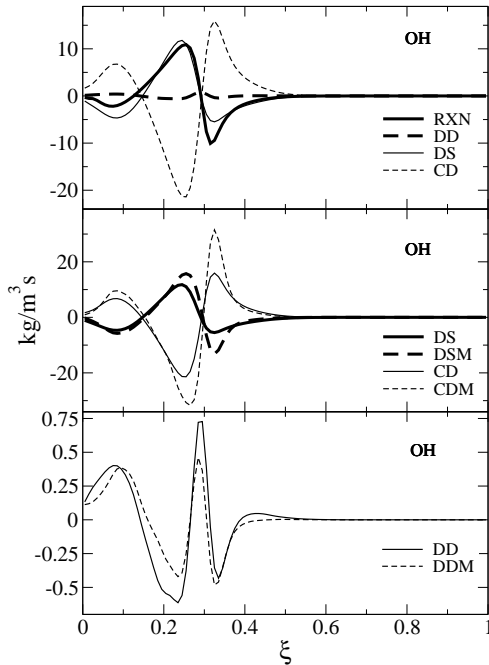


Figure 8: Plots of exact and modeled CMC terms for OH .

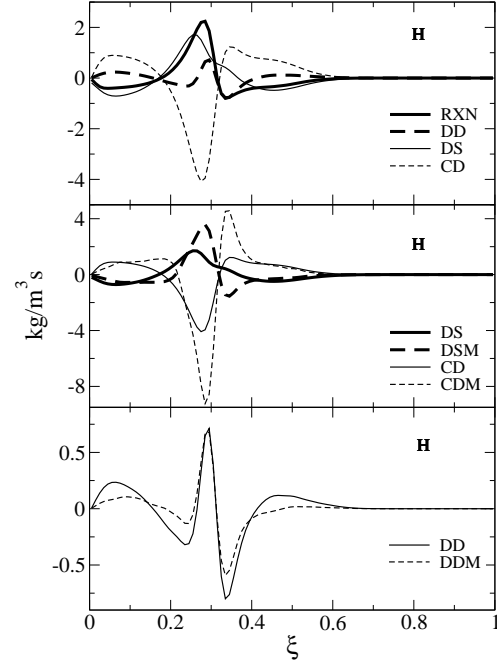


Figure 9: Plots of exact and modeled CMC terms for H .

dinate, hence all terms are important to the CMC transport equation of the given species. The differential diffusion term is quite small for OH , but significant for CO_2 and H . The cross-dissipation and dissipation-scalar terms tend to oppose and balance one another for each of the species throughout most of the mixture fraction domain, as previously observed [6].

A comparison of the exact and modeled CMC terms is given in the middle and lower plots of Figs. 7, 8, and 9 for species CO_2 , OH , and H , respectively. For each species, the center plot contains the dissipation-scalar and cross-dissipation terms, along with their modeling closures. The lower plots shows the differential diffusion term and its model. The DS and CD models show the right trend for each of the species, and reasonably good quantitative agreement for species CO_2 and OH . The modeled CS and DS terms do not agree as well for hydrogen, however.

The DD term and its model similarly show a good qualitative trend over the mixture fraction domain for each of the species, and the two curves are reasonably close in magnitude. The discrepancies between the modeled and exact terms are due to the neglect of cross correlations between the products of quantities making up the terms since this assumption is made in deriving the modeled terms. The model for the differential diffusion term of gaseous species, DDM in Eq. (8) is remarkably accurate, in contrast to the soot mass

fraction, and the model for the residual of the differential diffusion of the gaseous species is not required.

5. Summary and Conclusions

We have performed direct numerical simulations of a three-dimensional, planar, turbulent ethylene jet flame with soot formation. An a-priori analysis of a recent formulation of the CMC model for soot formation, specifically treating differential diffusion, has been performed. A common assumption neglecting spatial dependence of conditional quantities in the jet cross-stream direction has been made. The remaining CMC terms and proposed modeling closures for these terms have been extracted from the DNS for soot mass fraction and three gaseous combustion species. These results show that for soot mass fraction, the thermophoretic diffusion term is of secondary importance to the other CMC terms considered. The differential diffusion term is directly responsible for transport of soot in the mixture fraction coordinate. As the location of soot in the mixture fraction space dictates its temperature, and hence its reactivity and radiative properties, accurate modeling of this term is important. The modeling approximations for the soot differential diffusion are shown to have the right qualitative trend, and to be in reasonable quantitative agreement with the exact differential diffusion term.

Differential diffusion is also observed to be significant for gaseous species. CMC terms representing turbulent cross-dissipation between the species mass fractions and the mixture fraction, a dissipation-scalar term, the reaction source term and the differential diffusion term are shown to be of similar magnitude. The modeling of the cross-dissipation and dissipation-scalar resulted in overshoot, while the differential diffusion model terms are observed to be reasonably accurate.

Acknowledgments

This work was supported by the U. S. Department of Energy, Office of Basic Energy Sciences, Division of Chemical Sciences, Geosciences, and Biosciences. Simulations were performed at Sandia National Laboratories on the Redstorm supercomputer. Sandia National Laboratories is a multiprogram laboratory operated by Sandia Corporation, a Lockheed Martin Company, for the United States Department of Energy under contract DE-AC04-94-AL85000.

References

- [1] A. Y. Klimenko, R. W. Bilger, *Progress in Energy and Combustion Science* 25 (1999) 595–687.
- [2] R. W. Bilger, *Physics of Fluids A* 5 (1993) 436–444.
- [3] A. Kronenburg, R. W. Bilger, *Physics of Fluids* 9 (1997) 1435–1447.
- [4] A. Kronenburg, R. W. Bilger, J. H. Kent, *Combustion and Flame* 121 (2000) 24–40.
- [5] Yunardi, R. M. Woolley, M. Fairweather, *Combustion and Flame* 152 (2008) 360–376.
- [6] J. Hewson, A. Ricks, S. Tieszen, A. Kerstein, R. Fox, Conditional moment closure with differential diffusion for soot evolution in fire, in: *Center for Turbulence Research, Proceedings of the Summer Program, 2006*.
- [7] C. A. Kennedy, M. H. Carpenter, R. M. Lewis, *Applied Numerical Mathematics* 35 (3) (2000) 177–219.
- [8] C. A. Kennedy, M. H. Carpenter, *Applied Numerical Mathematics* 14 (4) (1994) 397–433.
- [9] R. J. Kee, F. M. Rupley, J. A. Miller, *Chemkin, Reaction Design, Inc., San Diego CA* (2000).
- [10] R. J. Kee, G. Dixon-Lewis, J. Warnatz, M. E. Coltrin, J. A. Miller, H. K. Moffat, *Transport, Reaction Design, Inc., San Diego CA* (2000).
- [11] D. O. Lignell, J. H. Chen, P. J. Smith, T. Lu, C. K. Law, *Combustion and Flame* 151 (1-2) (2007) 2–28.
- [12] K. M. Leung, R. P. Lindstedt, *Combustion and Flame* 87 (1991) 289–305.
- [13] S. E. Pratsinis, *Journal of Colloid and Interface Science* 124 (2) (1987) 416–427.
- [14] J. C. Sutherland, C. A. Kennedy, *Journal of Computational Physics* 191 (2003) 502–524.
- [15] R. W. Bilger, S. H. Starner, R. J. Kee, *Combustion and Flame* 80 (2) (1990) 135–149.
- [16] A. Kronenburg, M. Kostka, *Combustion and Flame* 143 (2005) 342–356.
- [17] D. O. Lignell, J. H. Chen, P. J. Smith, Three-dimensional direct numerical simulation of soot formation and transport in a temporally-evolving non-premixed ethylene jet flame, *Combustion and Flame*, accepted for publication May 13, 2008.
- [18] M. J. Cleary, J. H. Kent, *Combustion and Flame* 143 (2005) 357–368.